Journal of Sol-Gel Science and Technology (2020) 94:477–485
https://doi.org/10.1007/s10971-020-05263-6

ORIGINAL PAPER: NANO-STRUCTURED MATERIALS (PARTICLES, FIBERS, COLLOIDS, COMPOSITES, ETC.)

Check for updates

Ultrasonic-assisted sol–gel synthesis of TiO_2 nanostructures: Influence of synthesis parameters on morphology, crystallinity, and photocatalytic performance

Y. Quintero[1] · E. Mosquera[2,3] · J. Diosa[2,3] · A. García[1]

Received: 3 December 2019 / Accepted: 21 February 2020 / Published online: 5 March 2020

Abstract

The influence of synthesis parameters using the ultrasonic-assisted sol–gel method on the properties of TiO_2 nanostructures was studied. Different synthesis conditions such as long stirring time, type of acid used as the catalyst (weak or strong acid), and calcination temperature were explored and their influences on the morphology, size, crystallinity of nanostructures, and photocatalytic performance were evaluated. TiO_2 nanostructures were characterized by Fourier transform infrared spectroscopy, transmission electron microscopy, X-ray diffraction, and ultraviolet–visible diffuse reflectance spectroscopy. Moreover, degradation photocatalytic tests were performed using methylene blue as the polluting model. Changes in the morphologies and sizes of nanostructures were observed by modification of the stirring time using this sonication process. Moreover, the use of a weak acid, such as acetic acid, produced nanostructures with higher anatase proportion, larger crystallite size, and larger nanoparticle size compared with the use of a strong acid such as nitric acid. In addition, changes in crystalline phases were observed with an increase in the calcination temperature. Finally, the photocatalytic performance was influenced mainly by the changes in the crystalline phases, which were dependent on the type of acid catalyst and the calcination temperature.

Graphical Abstract

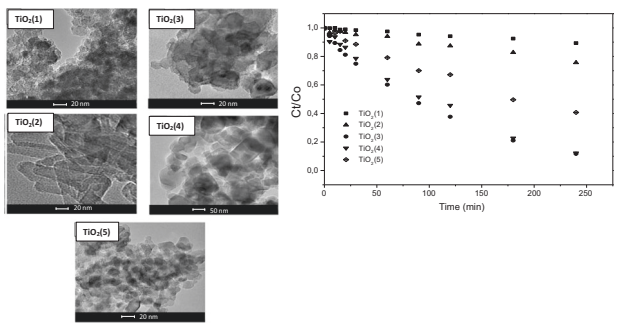

Supplementary information The online version of this article (https://doi.org/10.1007/s10971-020-05263-6) contains supplementary material, which is available to authorized users.

✉ A. García
andreina.garcia@amtc.cl

[1] Advanced Mining Technology Center, Universidad de Chile, Beauchef 850, Santiago, Chile

[2] Departamento de Física, Universidad del Valle, Cali A.A. 25360, Colombia

[3] Centro de Excelencia en Nuevos Materiales, Universidad del Valle, Cali A.A. 25360, Colombia

Keywords TiO_2 nanostructures · Sol–gel · Ultrasonic stirring · Acid catalyst · Photocatalysis

Highlights

- Synthesis parameters of TiO_2 nanostructures by the sol–gel method are investigated.
- Ultrasonic stirring time, acid type as a catalyst and calcination temperature are evaluated.
- Morphology, size, crystallinity, and photocatalytic performance of nanostructures are studied.
- Ultrasonic stirring time affect the morphology and the size of nanostructure.
- Acid type and calcination temperature influence on crystalline phases and nanoparticle size.
- Photocatalytic performance is mainly influenced by the change in the crystalline phases.

1 Introduction

Titanium dioxide (TiO_2) is one of the most studied semiconductors due to its many favorable properties, including high chemical and physical stabilities, non-toxicity, good electrical properties, and great optical properties [1–3]. These characteristics have facilitated a wide spectrum of applications, such as pigments, filters, catalyst supports, gas sensors, photocatalysts, destruction of microorganisms, such as bacteria and viruses, degradation of organic pollutants, inactivation of cancer cells, control of odors, self-cleaning surfaces, and solar cells [4–12]. In this regard, it has been widely reported that the properties of TiO_2 are strongly related to its morphology, size, crystal phases, and others [2–6].

Four crystalline phases of titanium dioxide have been reported: anatase and rutile with a tetragonal arrangement, brookite with an orthorhombic crystal lattice, and a new monoclinic structure known as TiO_2 (B) [13, 14]. The anatase and rutile phases have high physical stability, in contrast to the other phases, which are considered metastable phases. Rutile is commonly used for white pigments and coatings due to its great refractivity. Better photocatalytic properties are associated with the anatase structure [15].

Thus, to produce nanomaterials with specific properties, different synthesis routes, such as sol–gel, solvothermal, hydrothermal, mechanical alloying, and laser ablation routes, have been reported [16–25]. However, synthesis by the sol–gel route stands out because it is a simple method of preparation of TiO_2 nanoparticles and has low production cost [26–28].

Synthesis via the sol–gel method consists of the hydrolysis and posterior condensation of metal alkoxides in aqueous media. In the presence of water, alkoxides are hydrolyzed and subsequently polymerized through nucleation and growth processes, which occur very rapidly, and tridimensional oxide particles are eventually formed. However, the products obtained via the sol–gel process have low crystallinity, thus allowing a relevant subsequent heat treatment process to promote crystallinity and selectivity of the crystalline phases of the nanoparticles [1, 13, 29].

The synthesis conditions, such as the type of precursor, molar ratio of water/precursor, type of acid used as a catalyst, of TiO_2 nanoparticles by sol–gel have been studied to improve the nanoparticle properties [1, 14, 30].

Another relevant condition to be considered during synthesis by the sol–gel route is the stirring process. This process could influence the characteristics of the nanostructures, such as their morphology, size, and crystal phases [31–33]. Thus, the type and time of stirring of this synthesis method cannot be a trivial issue. Extensive studies pertaining to the synthesis of TiO_2 nanoparticles by the sol–gel method by means of magnetic stirring have been conducted [1, 14, 15]. However, few studies have explored the use of other types of stirring, such as ultrasonic stirring.

In this last regard, some initiatives have been reported. For example, Arunmetha et al. produced TiO_2 nanoparticles from natural rutile sand using different approaches, such as sol–gel, sonication, and spray pyrolysis [31]. They compared the particle sizes, crystalline structures, surface areas, morphologies, and energy band gaps of the nanoparticles produced and obtained decreases in particle size and increases in energy band gap and surface area when the process was changed from sol–gel to sonication and from sonication to spray pyrolysis. Nevertheless, in this case, the influence of stirring time on these properties was not considered. On the other hand, Xia et al. studied the effect of stirring time for ultrasonic stirring in the synthesis of TiO_2 nanoparticles using $TiCl_4$ as the precursor [32]. They evaluated two stirring times, 30 and 60 min, and obtained an increase in particle size by increasing the stirring time. Moreover, specific morphologies, including TiO_2 nanorods and rutile single phase were obtained. On the contrary, Neppolian et al. observed a different behavior. They also compared stirring times (30, 60, 90, and 120 min) for an ultrasonic-assisted sol–gel method and evaluated their influences on the morphology of the TiO_2 nanoparticles. Moreover, two different types of ultrasonic stirring, bath type and tip type, were explored [33]. However, a clear tendency on the morphological parameters, such as crystalline size, pore volume, and pore size, was not observed with increase in the stirring time. Moreover, slight

differences in percentages of crystalline phases of nanoparticles prepared by the different types of source stirring were observed.

Based on the above, the influences of long ultrasonic stirring times by this synthesis route on the characteristics of the nanostructures, such as morphology, size, and crystal phases, remain unclear. Finally, another relevant synthesis parameter to explore in the sol–gel synthesis of TiO_2 nanoparticles under ultrasonic stirring is the impact of the acid catalyst. It has been reported that it accelerates the hydrolysis process of the alkoxide [15], thus influencing the properties of TiO_2 nanoparticles.

For example, previous studies have demonstrated that the variation of pH and type of catalyst for the sol–gel method under classic magnetic stirring affect the size and crystalline structure of the final particle. Mahshid et al. reported the dependence of the particle size related to the pH of the media, obtaining smaller particles with more acidic pH when the precursor was titanium isopropoxide (TTIP) [1]. Meanwhile, Sayilkan et al. compared the synthesis of TiO_2 nanoparticles using the sol–gel method with TTIP as the precursor and HCl as the acid catalyst [29]. They observed a strong relationship between the concentration of the HCl and the formation of the anatase crystal phase. In addition, Miki Kanna et al. studied the effect on the formation of crystal phases of TiO_2 nanoparticles synthetized by sol–gel with $TiCl_4$ as the precursor using different acids as the hydrolysis catalyst and obtained mostly amorphous titanium dioxide with the presence of anatase and rutile phases in most of the cases [15]. On the other hand, Andrade-Guel et al. synthesized TiO_2 by microwave assisted sol–gel using TTIP as the precursor and studied the effect of two acids as the catalyst on the phase transformation [30], demonstrating the important influence of the acid catalyst on crystalline phases.

Based on the aforementioned results, the synthesis of TiO_2 nanostructures using sol–gel assisted by ultrasound agitation with TTIP as the precursor and different types of acid catalysts represents an alternative synthesis route meriting exploration. Thus, the objectives of this work were to study the influences of synthesis parameters, including long stirring times, weak and strong acids as the catalyst, and calcination temperature, on the morphology, size, and crystallinity of nanostructures and their impact on the photocatalytic performance for the degradation of a model pollutant, methylene blue.

2 Materials and experimental procedure

2.1 Materials

All of the reagents were analytical grade and required no additional purification. Nitric acid (HNO_3), acetic acid (CH_3–COOH), ammonium hydroxide (NH_4OH), titanium (IV) isopropoxide, methylene blue (MB), and isopropanol were purchased from Sigma Aldrich.

Table 1 Summary of synthesis conditions of TiO_2 nanostructures

Sample	Agitation time (h)	Acid type	Calcination temperature (°C)
TiO_2 (1)	6	HNO_3	400
TiO_2 (2)	3	HNO_3	400
TiO_2 (3)	3	HNO_3	550
TiO_2 (4)	3	Acetic	550
TiO_2 (5)	3	Acetic	400
TiO_2 (N)	3	HNO_3	WC
TiO_2 (A)	3	Acetic	WC

WC without calcination

2.2 Synthesis

A simple synthesis using the sol–gel method was performed. Conventional sonication by magnetic stirring was modified by a more energetic type of stirring, ultrasonic stirring, and the effect of sonication time was studied. In addition, the variations of using two types of acids (nitric and acetic) and different calcination temperatures were evaluated.

The acidic solution (pH = 2) was obtained by the dilution of nitric acid or acetic acid with ammonium hydroxide in deionized water. A TTIP solution in isopropanol (25% v/v) was added to the acidic solution under continuous ultrasonic stirring. This solution was kept at 70 °C under ultrasonic stirring for different times (6 or 3 h). A TiO_2 colloid suspension was obtained. Finally, the colloid suspension was dried at 60 °C for 20 h to obtain a powder sample, and the subsequent calcinations at different temperatures (400 and 550 °C) for 2 h were performed.

Different conditions of agitation time, acid type, and calcination temperature (°C) were used to study their influences on the properties of the nanostructures. Table 1 shows the synthesis conditions of the different samples.

2.3 Characterization of solids

Characterization of the TiO_2 nanostructures was performed. Fourier transform infrared (FTIR) measurements were conducted using a spectrophotometer (Rayleigh WQF-510A). The powders were mixed with KBr in a 5% (w/w) mixture. The mixed powder was pressed into tablets with a diameter of 1 cm at 10 tons for 1 min. The transparent tablets were inserted into the apparatus, and the spectra were recorded from 4000 to 400 cm^{-1} with a resolution step of 5 cm^{-1}. The KBr reference spectrum and CO_2 from the

ambient conditions were subtracted from every spectrum to verify the functional surface groups present in the TiO_2 nanostructures.

To determinate the crystalline phases, X-ray diffraction (XRD) patterns of the nanostructures were measured in the range of 0–90° using a Bruker D8 diffractometer with reflection mode (CuKα radiation source operated at 40 kV/30 mA). To estimate the percentages of crystalline phases, Rietveld refinement was realized. In addition, the mean size of crystallites (S) was obtained by Scherrer's formula [34, 35]. The morphology of the TiO_2 nanoparticles was examined by transmission electron microscopy (TEM) analysis (Tecnai F20 FEG-S/TEM) at 200 kV. Finally, ultraviolet–visible diffuse reflectance spectra (UV–vis/DRS) of the samples were obtained using a Lambda 1050 Wideband UV–Vis–NIR spectrometer equipped with a diffuse reflectance attachment (Biconical DRA-CA-50M) to estimate the energy band gap of the nanoparticles using the Kubelka–Munk function [36].

2.4 Photocatalytic tests

Photocatalytic tests were performed using a batch photoreactor. Irradiation was provided by a UV light lamp (Blak-Ray®, 100 W, 230 V, 365 nm). The tests were performed at 25 °C using 1 g/L of TiO_2 added under stirring into 200 ml of a solution of 5 ppm MB. The samples were maintained in the dark for 60 min in order to complete the adsorption at equilibrium prior the UV irradiation and then the suspension was irradiated. After centrifugation, MB aliquots were analyzed using a UV-spectrophotometer (Rayleigh Model UV1800 V/VIS–Spectrophotometer) at 664 nm, and the MB concentrations were estimated using a standard calibration curve. Photoactivity tests were done in triplicate for all samples, and the reproducibility of results was >3%.

3 Results and discussion

3.1 Influence of synthesis parameters on properties of the TiO_2 nanostructures

The influence of the sol–gel synthesis parameters assisted by ultrasound agitation on the properties of the TiO_2 nanostructures is presented here. The synthesis conditions, stirring time, type of acid catalyst (weak or strong), and calcination temperature, were considered and their impacts on the properties of the nanostructures, including morphology, size, and crystallinity, were analyzed.

3.1.1 Morphology

Figure 1 shows TEM images of the synthesized nanostructures. With regard to the impact of stirring time on this property, the figure shows that TiO_2(1) synthesized under 6 h of ultrasonic stirring exhibited particle sizes of around 10 nm in diameter (Fig. 1a). In contrast, nanoparticles synthesized under 3 h of ultrasonic stirring exhibited a combination of nanoparticle and nanorod morphologies (TiO_2(2), Fig. 1b). In this case, the nanoparticles had a size of ~10 nm, whereas the nanorods exhibited lengths larger than 20 nm.

Changes in ultrasonic stirring time affected the morphology of the nanostructures according to previous reports [32, 37]. This process produced high kinetic energy in the solution's motion, generating elastic, and inelastic collisions

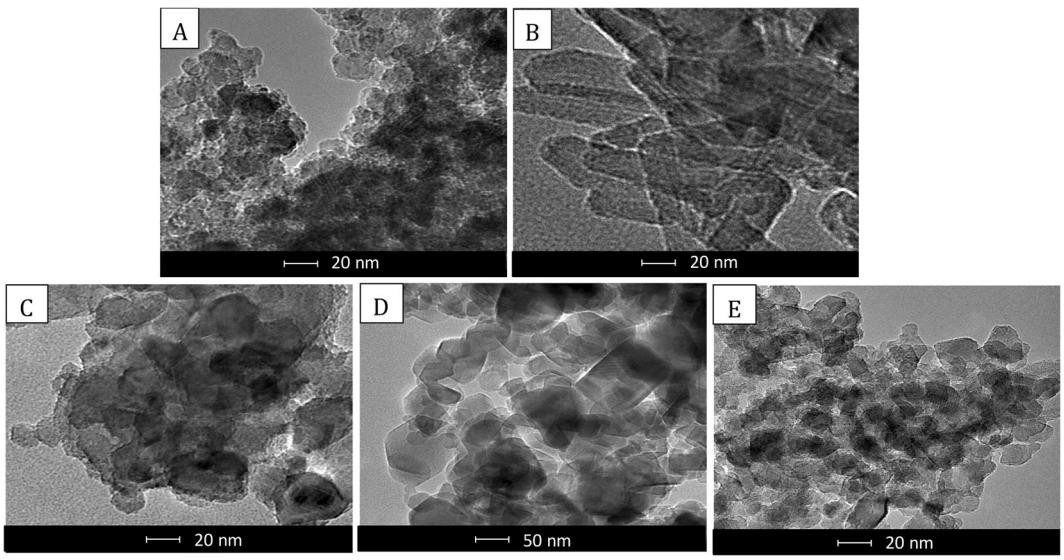

Fig. 1 TEM images of nanostructures: **a** TiO_2(1), **b** TiO_2(2), **c** TiO_2(3), **d** TiO_2(4), and **e** TiO_2(5)

in the colloidal suspension that initially induced implosive collapses, which favored the formation of structural arrays [38, 39]. Subsequently, the largest particles continued the collisions, which broke the structure into the smallest particles. This fact confirms the relation between ultrasonic stirring time and the morphology and size of particles [40].

On the other hand, when examining the influence of the type of acid catalyst, an interesting behavior was observed. The $TiO_2(4)$ sample synthesized by using acetic acid exhibited nanoparticles with a diameter of ~50 nm (Fig. 1d); however, $TiO_2(3)$ synthesized using nitric acid showed nanoparticles with a diameter of ~20 nm (Fig. 1c). This fact indicates that the use of a strong acid catalyst, such as nitric acid, promotes the formation of smaller nanoparticles, whereas a weak acid, such as acetic acid, favors larger nanostructures.

The influence of the type of acid catalyst in the sol–gel process can be explained. The preparation of metallic oxides in an aqueous medium by sol–gel occurs through the hydrolysis and subsequent condensation of alkoxide as follows [1]:

$$\mathrm{Ti(OR)_4 + 4H_2O \rightarrow Ti(OH)_4 + 4ROH\ (hydrolysis)}$$

$$\mathrm{Ti(OH)_4 \rightarrow TiO_2xH_2O + (2 - x)H_2O\ (condensation)},$$

where R is *ethyl*, *i-propyl, n-butyl*, etc., and *x* is the number of water molecules present in the medium. The time rate of hydrolysis and condensation is favored by the acid catalyst type [15]. The first phenomenon can be favored by a strong acid (acid with high dissociation constant (pKa)), such as nitric acid, which rapidly breaks the $Ti(OR)_4$ molecule. However, this type of acid can disfavor the condensation process, delay nucleation, and disfavor the growth of the nanostructure, generating nanoparticles of smaller size. Previous work with $TiCl_4$ as the precursor showed that the presence of a strong acid generates intermediaries that interfere in the condensation process, thus affecting the growth of the structure [15]. In contrast, with a weak acid such as acetic acid, hydrolysis could be achieved without affecting the processes of condensation and growth and larger particles could be obtained.

Finally, regarding the influence of the calcination temperature, Fig. 1d, e shows TiO_2 (4) and TiO_2 (5), treated at 550 and 400 °C, respectively. An increase in calcination temperature favors an increase in the size of the nanoparticles, which is attributable to the influence of the thermal treatment on the growth of the crystalline lattice of the nanostructure, which could promote changes in the crystalline phases. This fact has been widely studied in previous reports [1, 34, 41].

From the above, it is possible to state that the ultrasonic stirring time, type of acid, and calcination temperature in the synthesis process affect the morphology and size of the nanostructures, which highlights the relevance of controlling these synthesis parameters.

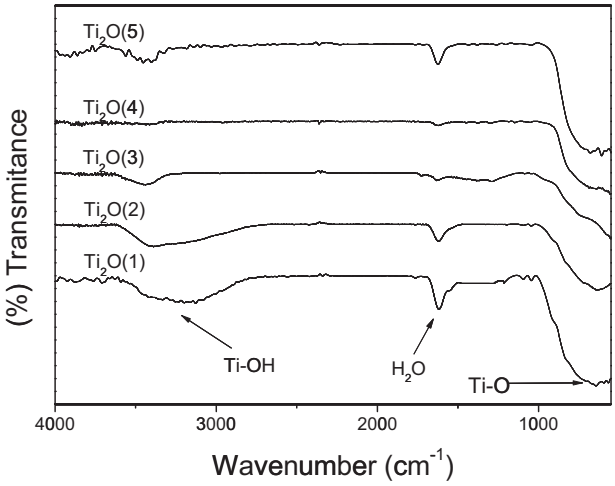

Fig. 2 FTIR spectra of the TiO_2 nanostructures

3.1.2 Surface chemistry

Figure 2 shows FTIR spectra of TiO_2 nanostructures synthesized under different conditions of agitation time, acid type, and calcination temperature, which are also described in Table 1.

In summary, no significant changes in spectra were observed despite the changes in synthesis conditions. In general, a broad peak identified as the bulk titania framework and attributable to the vibrational modes of the metal-oxide bonds associated with the Ti–O and Ti–O–Ti stretching modes can be seen in the region from 400 to 880 cm^{-1}, which confirms the formation of titanium dioxide in all samples [31, 42]. In addition, there are bands around 1620 and 3410 cm^{-1}, which are attributable to the deformation modes of water molecules and the stretching modes of –OH groups present in the samples due to possible reabsorption of water from the environment [43].

3.1.3 Crystalline phases

Figure 3 shows XRD patterns of samples obtained before and after the calcination processes (Fig. 3a, b). Table 2 shows the percentages of the crystalline phases obtained through Rietveld analysis.

A preliminary study of the sub-product obtained before the calcination process using sol–gel synthesis assisted by ultrasound agitation with acetic acid and nitric acid catalysts was conducted, and XRD patterns are shown in Fig. 3a. Despite the low crystallinity, small size crystallites

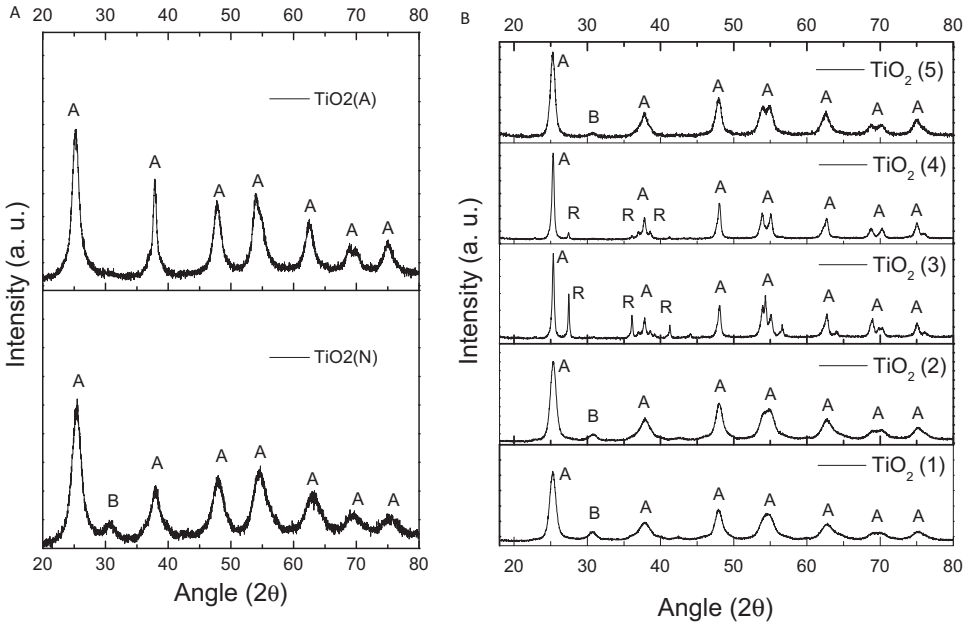

Fig. 3 XRD patterns of (**a**) precalcination nanostructures synthesized using acetic acid, TiO_2(A) and nitric acid TiO_2(N), and (**b**) TiO_2 nanostructures after calcination. A anatase, B brookite, R rutile

Table 2 Crystalline phases, crystallite size (S), and energy band gap (Eg) of TiO_2 nanostructures

Sample	Phases	% phases	S ± 0.1 (nm)	Eg (eV)
TiO_2 (1)	A-B	70-30	8.17	3.36
TiO_2 (2)	A-B	70-30	9.53	3.17
TiO_2 (3)	A-R	69-31	9.28	3.00
TiO_2 (4)	A-R	93-7	16.35	3.18
TiO_2 (5)	A-B	79-21	26.06	3.24
TiO_2 (N)	A-B	44-32	5.46	–
TiO_2 (A)	A	54	7.75	–

A anatase, *R* rutile, *B* brookite

No measured

associated with the spreading of the peak were observed [44, 45]. These showed main peaks at 2θ values corresponding to the anatase phase; however, brookite was observed in the sample prepared with nitric acid.

Postcalcination results are shown in Fig. 3b. In these cases, TiO_2 nanostructures show main peaks at 2θ values corresponding to the anatase phase; however, some differences in formation of crystalline phases associated with secondary peaks, such as for rutile and brookite, were observed, and these were dependent on the synthesis conditions.

Thus, the influence on the proportion of the crystalline phases associated with the catalytic acid type pre- and postcalcination processes was analyzed. Figure 3a shows higher anatase percentage in the presence of acetic acid (TiO_2(A)) as a catalyst than in the case with nitric acid (TiO_2(N)). Moreover, for the postcalcination samples, a higher anatase proportion occurred in presence of acetic acid (TiO_2(4) and TiO_2(5), 93 and 79%, respectively) than with nitric acid (TiO_2(1), TiO_2(2), and TiO_2(3)), around 70%). This confirms that acetic acid can favor the condensation process, nucleation, and the growth of the crystalline lattice, thus increasing the percentage of anatase. In contrast, in the presence of nitric acid, the condensation process could be limited, preventing growth of the crystalline lattice, so a lower percentage of anatase is obtained.

On the other hand, with regard to the influence of stirring time, no significant changes in crystalline phases were observed for TiO_2(1) with respect to TiO_2(2) synthesized under 6 and 3 h of ultrasonic stirring, respectively.

Moreover, it was also observed that TiO_2(1), TiO_2(2), and TiO_2(5), calcined at 400 °C, also exhibited a peak at 30.6°, which corresponds to the brookite phase; [2] whereas samples TiO_2(3) and TiO_2(4), calcined at 550 °C, showed peaks at 27.47°, 36.06°, and 41.26° corresponding to the rutile phase [35]. Thus, as has been widely reported, a high dependence on the formation of these crystalline phases with calcination temperature was observed [1, 34, 41].

3.1.4 Crystallite size

Table 2 shows the crystallite size of the TiO_2 nanostructures. It is important to note that the crystallite size is influenced mostly by the type of catalyst acid used in the synthesis process. Thus, when using an inorganic acid such as HNO_3, the average crystallite size was around 9 nm; however, when using an organic acid such as acetic acid, larger average crystallite sizes of around 21.2 nm were obtained.

3.1.5 Energy band gap

Figure 4 shows the UV–vis/DRS spectra of the TiO_2 nanostructures employed in the study of the optical properties of the samples after Kubelka–Munk function treatment [36, 46]. The optical energy band gaps of the prepared samples were analyzed by the intersection between the linear fit and the photon energy axis, and shifted band gap energy (Eg) values between 3.00 and 3.36 eV were observed for all nanostructures (Table 2). These values correspond to UV absorbance light of ~369 to 414 nm. Despite that, these energy band gap values are in agreement with previous reports and the standard commercial TiO_2 (3.22 eV for P25) [47].

3.2 Photodegradation effect

The kinetics of the photocatalytic disappearance of MB in the presence of TiO_2 nanostructures under a UV lamp were assessed (Fig. 5a). As can be seen from Fig. 5a, direct photolysis was negligible under UV irradiation. Assuming a first-order reaction rate, linear transformations (Fig. 5b) from the kinetic data were performed to estimate the apparent first-order rate constant [47]. Table 3 contains a summary of the kinetic results obtained for the MB photodegradation.

In this study, $TiO_2(3)$ and $TiO_2(4)$ exhibited the best photocatalytic performance with respect to the rest of the nanostructures, considering the higher rate of disappearance of the MB observed in the disappearance of kinetic data and the values of the apparently higher rate constants with respect to $TiO_2(1)$, $TiO_2(2)$, and $TiO_2(5)$. However, the $TiO_2(3)$ and $TiO_2(4)$ nanostructures did not attain the photocatalytic performance of a commercial standard TiO_2 (P25, Sigma-Aldrich) (see Supplementary Material).

In general, all of the nanostructures showed nanoscale sizes and behaviors consistent with those of a UV-photosensitive material. However, the $TiO_2(3)$ and $TiO_2(4)$ nanostructures presented anatase–rutile proportions, in contrast with the rest of the nanostructures that presented anatase–brookite proportions. This means that the photocatalytic performance is influenced mainly by the crystalline phases, as has been widely reported [41, 47].

Anatase has been reported as a phase with higher photocatalytic activity. In addition, control of the synthesis conditions to obtain a significant percentage of this phase and absence of the brookite phase could guarantee a photocatalyst with best performance in the photodegradation of MB under UV light.

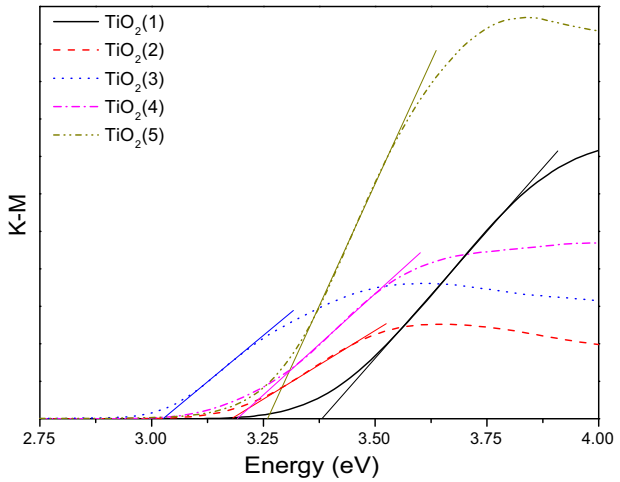

Fig. 4 UV–vis diffuse reflectance spectra of the TiO_2 nanostructures

4 Conclusions

TiO_2 nanostructures formed by the sol–gel method with ultrasound agitation using TTIP as the precursor and

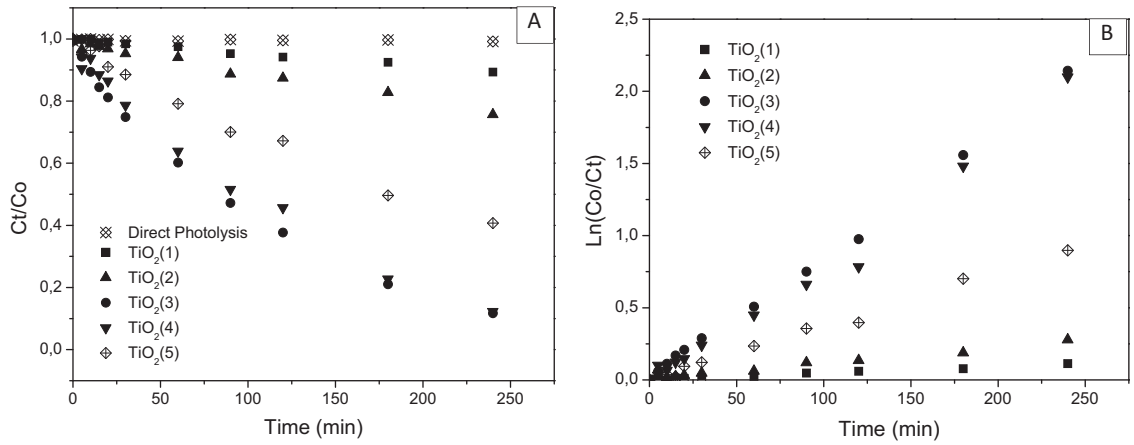

Fig. 5 Photodegradation of methylene blue (MB) on TiO_2 nanostructures under UV light. **a** Kinetics of disappearance of MB and (**b**) lineal regression of kinetic data

Table 3 Degradation kinetic constants (k), percentage degradation, and linearity constant R^2 of TiO_2 nanostructures in MB degradation

Sample	k (min^{-1})	R^2
TiO_2 (1)	0.5	0.9869
TiO_2 (2)	1.1	0.9837
TiO_2 (3)	8.7	0.9974
TiO_2 (4)	8.4	0.9856
TiO_2 (5)	3.7	0.9929

different types of acid catalysts (weak and strong acids) showed significant influences on their morphology, size, crystallinity, and photocatalytic performance.

The stirring time of the sonication process produced changes in the morphology and size of the nanostructures. The TiO_2 synthesized via 6 h of ultrasonic stirring exhibited nanoparticles, whereas the TiO_2 synthesized by using 3 h of ultrasonic stirring exhibited a combination of nanoparticle and nanorod morphologies.

Moreover, the crystallite and nanoparticle sizes and the percentage of anatase phase in the nanostructure were strongly associated with the type of catalyst acid used in the synthesis process. In the presence of a weak acid such as acetic acid, a higher anatase proportion, larger crystallite sizes, and larger nanoparticle sizes were observed than in the presence of a strong acid such as nitric acid. This fact was attributed to the influence of the acid on the condensation process, nucleation, and growth of the crystalline lattice.

All nanostructures exhibited nanoscale sizes and behaviors similar to those of a UV-photosensitive material. Thus, the photocatalytic performance was influenced mainly by the crystalline phases. In this way, the TiO_2(3) and TiO_2(4) nanostructures, which presented anatase and rutile phases with a high proportion of anatase (69:31 and 93:7, respectively), influenced by the synthesis parameters, such as the type of acid catalyst and the calcination temperature, showed the highest photoactivity for the degradation of MB.

Acknowledgements The authors gratefully acknowledge the financial support provided by the Fund for the Promotion of Scientific and Technological Development (FONDEF) of the Government of Chile (Project no. ID15I10086) and also acknowledge the Universidad de Santiago de Chile (USACH), especially Professor Diego Venegas-Yazigi for the UV–vis/DRS analysis.

Compliance with ethical standards

Conflict of interest The authors declare that they have no conflict of interest.

References

1. Mahshid S, Askari M, Ghamsari M (2007) Synthesis of TiO2 nanoparticles by hydrolysis and peptization of titanium isopropoxide solution. J Mater Process Technol 189:296–300
2. Lopez-Muñoz M, Revilla A, Alcalde G (2015) Brookite TiO2-based materials: synthesis and photocatalytic performance in oxidation of methyl orange and As(III) in aqueous suspensions. Catal Today 240:138–145
3. Afuyoni M, Nashed G, Nasser I (2011) TiO2 doped with SnO2 and studing its structurail and electrical properties. Energy Procedia 6:11–20
4. García A, Quintero Y, Vicencio N, Rodríguez B, Ozturk D, Mosquera E, Corrales TP, Volkmann UG (2016) Influence of TiO2 nanostructures on anti-adhesion and photoinduced bactericidal properties of thin film composite membranes. RSC Adv 6:82941–82948
5. Liu J, Li Y, Arumugam S, Tudor J, Beeby S (2018) Investigation of low temperature processed titanium dioxide (TiO2) films for printed dye sensitized solar cells (DSSCs) for large area flexible applications. Mater Today 5:13846–13854
6. Omprakash S, Kumar S, Holla R (2018) Titanium dioxide and Zinc oxide as a dielectric material for application in TFT's. Mater Today 5:10833–10838
7. H. Memon, S. Yasin, N. Khoso, M. Hussain (2015) Indoor decontaminating textiles by photo catalytic oxidation—a review. J Nanotech 2015:1–9
8. Memon H, Kumari N (2016) Study of multifunctional nanocoated cold plasma treated polyester cotton blended curtains. Surf Rev Lett 5:1–11
9. Chen W, Yu J, Hu W, Chen Z, Memon H, Chen G (2016) Titanate nanowires/NiO nanoflakes core/shell heterostructured nanonanocomposite catalyst for the methylene blue photodegradation. RSC Adv 72:67827–67832
10. Saini A, Sharma J, Sharma R, Chaudhary A, Sharma D, Dhayal V (2019) Zinc oxide derived from zinc(II)/acetoxime system: formation pathway and solar-driven photocatalytic and antimicrobial applications. J Sol-Gel Sci Technol 91:644–653
11. Memon H, Kumari N, Jatoi A, Khoso N (2016) Study of the indoor decontamination using nanocoated woven polyester fabric. Int Nano Lett 7:1–7
12. Baradaran M, Ghodsi F (2019) Highly efficient visible photocatalytic degradation of MB organic dye by heteromorphic ZnO/AZO/ZnO nanocatalysts: effect of AZO thickness. J Sol–Gel Sci Technol 92:25–39
13. Dubey R (2018) Temperature-dependent phase transformation of TiO2 nanoparticles synthesized by sol-gel method. Mater Lett 215:312–317
14. Imran M, Riaz S, Naseem S (2015) Synthesis and characterization of titania nanoparticles by sol-gel technique. Mater Today 2:5455–5461
15. Kanna M, Wongnawa S (2008) Mixed amorphous and nanocrystalline TiO2 powders prepared by sol–gel method: characterization and photocatalytic study. Mater Chem Phys 110:166–175
16. Jongprateep O, Puranasamriddhi R (2018) Effects of reagents on the formation of nanoparticulatetitaniumdioxide synthesized by sol-gel technique. Mater Today 5:10925–10931
17. Ma Z, Jiang Y, Xiao H, Jiang B, Zhang H, Peng M, Dong G, Yu X, Yang J (2018) Sol-gel preparation of Ag-silica nanocomposite with high electrical conductivity. Appl Surf Sci 436:732–738
18. Kong F, Ning W, Wang A, Liu Y, Tian M (2018) Convenient solvothermal synthesis of nanoscale 0-2D Bi without surfactants and templates. J Alloy Compd 737:484–489
19. Bincy J, Silvena G, Rajesh A (2018) Influence of reaction time on the structural, optical and electrical performance of copper antimony sulfide nanoparticles using solvothermal method. Phys B 537:243–250

20. Meng L, Wang B, Ma M, Lin K (2016) The progress of microwave-assisted hydrothermal method in the synthesis of functional nanomaterials. Mater Today Chem 1:63–83
21. Peng T, Ray S, Veeravalli S, Lalman J, Arefi F (2018) The role of hydrothermal conditions in determining 1D TiO2 nanomaterials bandgap energies and crystal phases. Mater Res Bull 105:104–113
22. Goyal A, Soni P (2018) Functionally graded nanocrystalline silicon powders by mechanical alloying. Mater Lett 214:111–114
23. Rabiee M, Mirzadeh H, Ataie A (2017) Processing of Cu-Fe and Cu-Fe-SiC nanocomposites by mechanical alloying. Adv Powder Technol 28:1882–1887
24. Tan D, Zhou S, Qiu J, Khusro N (2013) Preparation of functional nanomaterials with femtosecond laser ablation in solution. J Photochemistry Photobiol C 17:50–68
25. Xiao J, Liu P, Wang C, Yang G (2017) External field-assisted laser ablation in liquid: An efficient strategy for nanocrystal synthesis and nanostructure assembly. Prog Mater Sci 87:140–220
26. Pelaez M, Nolan N, Pillai S, Seery M, Falaras P, Kontos A, Dunlop P, Hamilton J, Byrne J, O'Shea K, Entezari M, Dionysiou D (2012) A review on the visible light active titanium dioxide photocatalysts for environmental applications. Appl Catal B 125:331–349
27. Mahy J, Deschamps F, Collard V, Jérôme C, Bartlett J, Lambert S, Heinrichs B (2018) Acid acting as redispersing agent to form stable colloids from photoactive crystalline aqueous sol–gel TiO2 powder. J Sol–Gel Sci Technol 87:568–583
28. Tian Q, Wei W, Dai J, Sun Q, Zhuang J, Zheng Y, Liu P, Fan M, Chen L (2019) Porous core-shell TixSn1-xO2 solid solutions with broad-light response: one-pot synthesis and ultrahigh photooxidation performance. Appl Catal B 244:45–55
29. Sayilkan F, Asiltürk M, Sayilkan H, Önal Y, Akarsu M, Apac E (2005) Characterization of TiO2 synthesized in alcohol by a sol-gel process: the effects of annealing temperature and acid catalyst. Turk J Chem 29:697–706
30. Andrade M, Díaz L, Cortés D, Cabello C, Ávila C, Bartolo P, Gamero P (2018) Microwave assisted sol–gel synthesis of titanium dioxide using hydrochloric and acetic acid as catalyst. Boletín de la sociedad Española de céramica y vidrio. https://doi.org/10.1016/j.bsecv.2018.10.005
31. Arunmetha S, Manivasakan P, Karthik A, Babu N, Srither S, Rajendran V (2013) Effect of processing methods on physicochemical properties of titania nanoparticles produced from natural rutile sand. Adv Powder Technol 24:972–979
32. Xia X, Luo Y, Wang Z, Liang Y, Fan J, Jia Z, Chen Z (2007) Ultrasonic synthesis and photocatalytic activity investigation of TiO2 nanoarrays. Mater Lett 61:2571–2574
33. Neppolian B, Wang Q, Jung H, Choi H (2008) Ultrasonic-assisted sol-gel method of preparation of TiO2 nano-particles: Characterization, properties and 4-chlorophenol removal application. Ultrason Sonochem 15:649–658
34. Li B, Wang X, Yan M, Li L (2002) Preparation and characterization of nano-TiO2 powder. Mater Chem Phys 78:184–188
35. Jenkins R, Snyder R (1996) Introduction to X-ray powder diffractometry. vol 138. Wiley, New York, NY
36. Kubelka P, Munk F (1931) An article on optics of paint layers. Tech Phys 12:593
37. Kenneth P, Suslick S, Gareth J (1999) Applicatios of ultrasound to materials chemistry. Annu Rev Mater Sci 29:295–326
38. ullah H, Khan I, Yamani Z, Qurashi A (2017) Sonochemical-driven ultrafast facile synthesis of SnO2 nanoparticles: Growth mechanism structural electrical and hydrogen gas sensing properties. Ultrason Sonochem 34:484–490
39. Mosquera E, Carvajal N, Morel M, Marín C (2017) Fabrication of ZnSe nanoparticles: structural, optical and Raman Studies. J Lumin 192:814–817
40. Mosquera E, Carvajal N (2014) Low temperature synthesis and blue photoluminescence of ZnS submicronparticles. Mater Lett 129:8–11
41. Alzamani M, Shokuhfar A, Eghdam E, Mastali S (2013) Influence of catalyst on structural and morphological properties of TiO2 nanostructured films prepared by sol–gel on glass. Prog Nat Sci 1:77–84
42. Naseem S, Riaz S (2015) Controlled nanostructuring of TiO2 nanoparticles: a sol-gel approach. J Sol–Gel Sci Technol 74:299–309
43. Mathew S, Kumar A, Benoy T, Rakesh P, Hari M, Libish T, Radhakrishnan P, Nampoori V, Vallabhan C (2012) UV-visible photoluminiscence of TiO2 nanoparticles prepared by hydrothermal method. J Fluoresc 22:1563–1569
44. Vinogradov A, Vinogradov V (2014) Effect of acidic peptization on formation of highly photoactive TiO 2 films prepared without heat treatment. J Am Ceram Soc 97:290–294
45. Malengreaux C, Pirard S, Léonard G, Mahy J, Herlitschke M, Klobes B, Hermann R, Heinrichs B, Bartlett J (2017) Study of the photocatalytic activity of Fe3+, Cr3+, La3+ and Eu3+ single-doped and co-doped TiO2 catalysts produced by aqueous sol-gel processing. J Alloy Compd 691:726–738
46. Reyes-Coronado D, Rodriguez-Gattorno G, Espinosa-Pesqueira ME, Cab C, de Coss R, Oskam G (2008) phase-pure TiO2 nanoparticles: anatase, brookite and rutile. Nanotechnology 19:145605
47. Matos J, Quintana K, García A (2012) Influence of H-type and L-type activated carbon in the photodegradation of methylene blue and phenol under UV and visible light irradiated TiO2. Mod Res Catal 1:1–9